IEEE Access
Multidisciplinary | Rapid Review | Open Access Journal

Received May 12, 2021, accepted June 3, 2021, date of publication June 7, 2021, date of current version June 21, 2021.

Digital Object Identifier 10.1109/ACCESS.2021.3087171

Multi-Physical Coupling Field of a Permanent Magnet Linear Synchronous Generator for Wave Energy Conversion

CHUNYUAN LIU, DONG RUI, HE ZHU, AND WENZHEN FU

College of Information Science and Engineering (College of Mechanical Engineering), Jiaxing University, Jiaxing 314000, China

Corresponding author: Chunyuan Liu (liuchunyuan_zjx@163.com)

This work was supported in part by the Zhejiang Provincial Natural Science Foundation of China under Grant LY19E070004, and in part by the Project of Jiaxing Science and Technology Bureau China under Grant 2019AD32025.

ABSTRACT Permanent Magnet Linear Synchronous Generators (PMLSG) has high power density and high efficiency, which is always employed in industrial application field. However, as temperature increases, it is easy to cause demagnetization of the permanent magnet, and the applications of PMLSG is limited. In this paper, a PMLSG is optimized which is used in a low speed power generation system. Firstly, a multi-physical coupling field system is described, and introduced the main factors which affecting the design of the PMLSM. Secondly, a multi-physics optimization method based on Genetic Algorithm (GA) is to improve the power density and efficiency. At the same time reduce the material cost of the generator. The thermal model is established and analysis the losses of PMLSG. The conductive heat transfer coefficient is calculated. Then, a Finite Element Analysis (FEA) model is established, and the electromagnetic properties of PMLSG were analyzed. The results of the electromagnetic field calculation are imported into the transient thermal analysis model by FEA, and the temperature of each part for PMLSG are calculated. Finally, an experimental test platform is built for verifying the correctness of the analysis.

INDEX TERMS Magnetic-thermal coupling analysis model, permanent magnet linear synchronous generator, finite element analysis, genetic algorithm.

I. INTRODUCTION

Permanent Magnet Linear Synchronous Generators (PMLSGs) which has high power density, high efficiency and high reliability are widely used in industrial field, especially in the direct-drive field. For example, wave power take-off system [1], [2], Computer Numerical Control (CNC) Machine [3], Linear Actuator [4] and other aspects of the application [5], [6]. The high demand and a wide application area, the PMLSG must be designed high efficiency and more energy efficient. The high demand for PMLSGs applications, the PMLSGs need to be designed very efficient, and this includes developments in the machine materials, optimization design, and manufacturing. Among them, optimization design is one of a key technology to improve the electromagnetic and mechanical properties for PMLSGs.

Nowadays, there are many methods on PMLSG optimization [7]–[9]. However, most methods are only optimized for only one or two parameters. Reference [10] only the end forces in LPMSGs are optimized. Reference [11] is mainly concerned with thrust density. Nowadays, the thermal analysis of permanent magnet motors is mainly focus on thermal circuit method [12], [13] and numerical calculation method [14], [15]. However, PMLSG which apply to energy conversion system is influenced by many factors such as mechanical strength, electromagnetic performance, temperature, *et al.* Therefore, it is necessary to combine the multi-physics to optimize design the PMLSG.

Heating and temperature rise have directly affected the motors performance, more serious is reduction of service life or damage the motors. Obviously, the temperature of PMLSG must be controlled within a certain range in the process of designing PMLSG. Therefore, how to accurate temperature rise has increasing significance on the design, manufacture, and application of linear motors. In this paper, the designed PMLSG is used in wave power take-off system, due to the complexity of the maritime environment, special design is required for the PMLSG. In this way, the costs of direct-drive

The associate editor coordinating the review of this manuscript and approving it for publication was Shaopeng Wu.

wave power generator system are increased, especially the cost of PMLSG. Therefore, one of the key researches is how to reduce the cost of PMLSG. In other words, how to optimize the design of PMLSG is very important for the direct-drive wave power generator.

Based on the previous works, in this paper, a multi-physics design optimization method based on Genetic Algorithm (GA) of PMLSG is presented to improve the utilization of the materials and the electromagnetic performance.

II. METHODOLOGY

Wave power take-off system is a multi-physical coupled-field system which include geometric sub-model, mechanical sub-model, electric sub-model, thermal sub-model, magnetic sub-model, and economic sub-model. This section describes the multi-physics design optimization for the direct-drive wave energy converter based on the PMLSG. The diagram of the wave energy converter is shown in Fig. 1, and the structure and variable parameters of the PMLSG are shown in Fig. 2. The outer-PM is chosen to convenient buoy installation. Quasi-Halbach magnetizing has a number of attractive characteristics, such as a sinusoidal back-electromotive force (back-EMF) waveform, which is conducive to very low electromagnetic force ripple, and the possibility of being optimized to achieve almost zero cogging force associated with both the slotting and the finite length of the stator core [16]. The parameters of wave are listed in Table 1, and the PMLSG parameters of initial design are listed in Table 2. Among them, the parameter of free stroke length is determined by the height of wave, and the parameter of the diameter of buoy is determined by the width of the experiment wave tank.

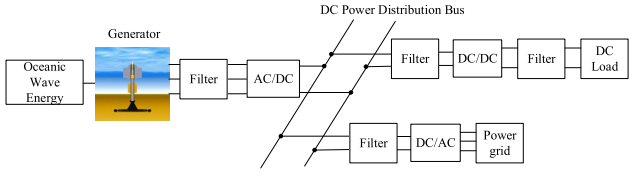

FIGURE 1. Diagram of the wave energy converter.

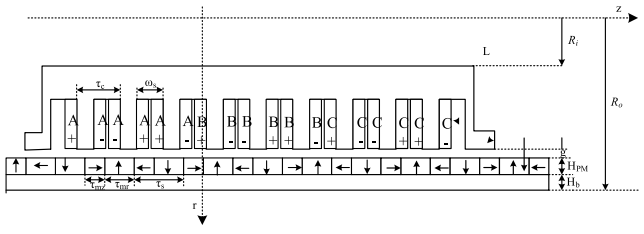

FIGURE 2. Structure and variable parameters of PMLSG.

The multi-physics design optimization (MDO) model is shown in Fig. 3. The sub-model is detailed in the following.

A. MECHANIC SUB-MODEL

The purpose of establishing the mechanic sub-model is to calculate the wave power energy available, and the wave

TABLE 1. Parameters of wave.

Parameters	Items	Value
L_{fsl}	free stroke length	0.4 m
v	speed of wave	0.6 m/s
D_b	diameter of buoy	0.8 m
H	height of wave	0.5 m

TABLE 2. PMLSG parameters of initial design.

parameters	items	value
τ_s	pole pitch	21.5 mm
τ_{mr}	length of radial permanent magnet	14.5 mm
τ_{mz}	length of axial permanent magnet	7 mm
τ_c	slot pitch	19.5 mm
ω_s	width of slot	10.5 mm
R_o	outer diameter	140 mm
R_i	inner diameter	54.5 mm
H_b	thickness of the back iron	3 mm
H_{PM}	thickness of the permanent magnet	3 mm
g	air-gap	3 mm
L	length of convex primary	18 mm
H_y	thickness of the yoke	13.5 mm
N	number of turns	120

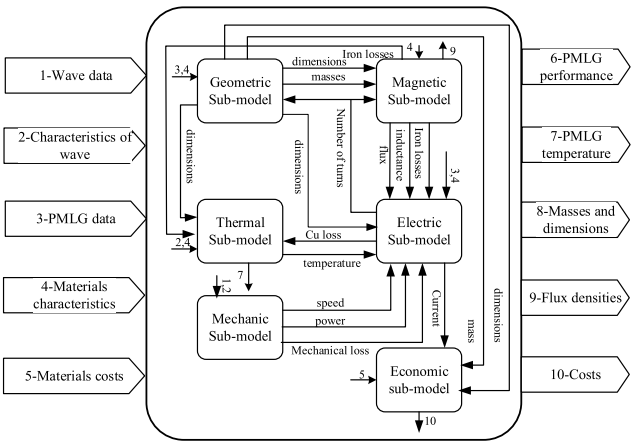

FIGURE 3. The multidisciplinary design model.

power per width (P_{mcl}) in real seals is

$$P_{mcl} = C_p \cdot \frac{\rho g^2 H_s^2 T_e}{64\pi} \approx C_p \cdot 491 \cdot H_s^2 T_e \qquad (1)$$

where C_p the wave power take-off system coefficient, ρ is the seawater density, and the value is considered as 1.025 kg/m^3, g is the acceleration of gravity, H_s is the significant wave height, and T_e is energy period.

B. GEOMETRIC SUB-MODEL

The geometric sub-model includes the structure of the PMLSG, the dimensions of various parts, the number of slots per pole and per phase, the number of poles, the number of turns. The materials characteristics which include enameled

wire, silicon steel sheet, and PMLSG shell. The output of geometric sub-model is the masses and volumes of the PMLSG. The main parameters are determined by the design method of traditional permanent magnet motor.

C. MAGNETIC SUB-MODEL

The purpose of the magnetic sub-model is to analysis the magnetic field performance of the PMLSG. The input parameters are the number of turns, the dimensions and messes, and the materials characteristics. The output parameters are the flux density, flux, inductances, iron losses.

D. THERMAL SUB-MODEL

The main aim of thermal Sub-model is to estimate the temperature in the permanent magnets to avoid demagnetization. The input parameters are iron losses, the dimensions, the copper and iron losses, characteristics of wave. The detail describe is show in the next part III.

E. ELECTRIC SUB-MODEL

The electric sub-model describes the analytical equations that express the electrical behavior of the PMLSG. The input parameters are the dimension, flux, inductance, iron losses, mechanical losses, PMLSG data (speed, power), and temperature. The outputs of the sub-model that include all the performance parameters of the PMLSG. This includes current, voltage, electromagnetic force, efficiency, the number of turns per coil (N_{tc}) and the required copper section per phase (S_{copper}).

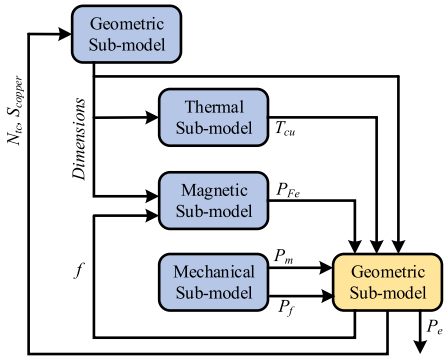

FIGURE 4. Block diagram to obtain the PMLSG output power.

The electric sub-model is interacted with other sub-models, and the output power of PMLSG is represented by a block diagram in Fig. 4. The interrelationships among these variables are described below.

1) The mechanical power (P_m) is obtained from the mechanical sub-model, and the its expression is shown as follow (2)

$$P_m = P_{mcl} \times W_{per\_width} \tag{2}$$

where W_{per_width} is per width of wave.

2) The friction losses that include air friction and mechanical friction losses. The air friction losses have a great relationship with the speed of machine [17], [18]. The design PMLSG is employed in wave energy conversions, it always works in a low speed conditions, therefore, the air friction loss is ignored in this paper.

3) The iron and copper losses are calculated by magnetic sub-model, which is discussed in more detail in the part III.

F. ECONOMIC SUB-MODEL

The purpose of this sub-model is to calculate the cost of PMLSG, which include the costs of permanent magnets (PMs), copper wire, silicon steel sheet and manufacturing cost. The mathematical formula of total cost (T_{cost}) is expressed as follow,

$$T_{cost} = PM_{cost} + Cu_{cost} + Steel_{cost} + Manufacturing_{cost} \tag{3}$$

where PM_{cost}, Cu_{cost}, and $Steel_{cost}$ are the cost of permanent magnet, coils, and steel, respectively.

In order to achieve high performance, the MDO of PMLSG must be investigated. The specific methods to achieve the following

Step 1: Definition of the PMLSG specifications which include the cost and output electromagnetic performance. The cost includes material cost and manufacturing cost. The output electromagnetic performance include power, efficiency, induced electromotive force (EMF), and other constraints, such as masses, volume, mechanical strength, and temperature rise, etc.

Step 2: Initial design. In order to acquire an initial design scheme, the materials, dimensions and manufacturing methods are researched in this step. For the materials of PMLSG, which include the PMs, steel, enameled wire, and motor shell. For the manufacturing method, the press method is recommended based on our design and prototyping experiences as it is widely used for batch production of PMLSG.

Step 3: Establish the multi-physics model for PMLSG. The magnetic sub-model, electric sub-model, thermal sub-model and mechanic sub-model evaluate the PMLSG performance parameters.

Step 4: Performance calculation. If the performances of the designed PMLSG are satisfactory in terms of design specifications, it can be taken as an initial design scheme and can be used in the later part of optimization.

III. MULTI-PHYSICS OPTIMIZATION METHOD AND THERMAL MODEL

A. MULTI-PHYSICS OPTIMIZATION METHOS AND THERMAL MODEL

In order to achieve high performance of the system, a multi-disciplinary optimization model based on GA is developed for the PMLSG in the form as the following

$$\begin{aligned} \min: f(x) &= \frac{T_{\text{cost}}}{C_o} + \frac{P_o}{P_{out}} \\ s.t.\ \ g_1(x) &= 0.90 - \eta \le 0 \\ g_2(x) &= 400 - P_{out} \le 0 \end{aligned}$$

$$g_3(x) = sf - 0.8 \leq 0$$
$$g_4(x) = T_{PM} - 80 \leq 0$$
$$g_5(x) = T_{coil} - 80 \leq 0 \quad (4)$$

where x is the vector of design parameters, C_o is the initial design cost, P_o is the initial output power, η and P_{out} are the generator's efficiency and output power, sf is the fill factor, T_{PM} and T_{coil} are the temperature rises in the PMs and windings, respectively. $g_1(x)$, $g_2(x)$, $g_3(x)$, $g_4(x)$, and $g_5(x)$ are the function that describe the efficiency, output power, fill factor, PM temperature, and coils temperature.

Genetic Algorithm (GA) is a computational model that simulates the natural evolution of Darwin's biological evolution theory and the biological evolution process of genetic mechanism. Because it is a general global algorithm, GA is uncomplicated in encoding technology and genetic operation (selection, crossover and mutation, etc.) [19]. It is a method to search for optimal solutions by simulating natural evolutionary processes and has powerful global searching. A key issue in GA programming is the selection of the fitness function to obtain the best solution to a problem. Fig. 5 shows the cost and efficiency optimization flowchart of PMLSG based on GA.

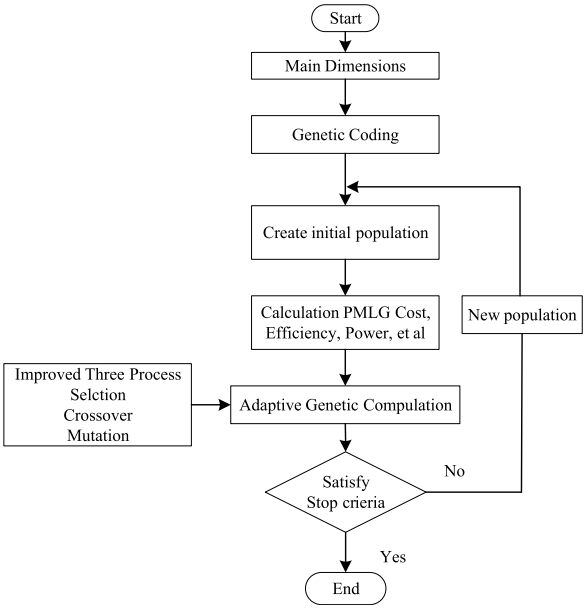

FIGURE 5. PMLSG cost and efficiency optimization flowchart based on GA.

The optimization flow diagram for PMLSG is shown in Fig. 6. G_o and P_o are the initial weight and power, respectively. G_i and P_i are the optimized weight and power, respectively. T_1 and T_2 are initial and optimized the temperature, respectively. ξ_1, ξ_2, and ξ_3 are the iterative residual.

In this paper, the optimization goals are the costs and efficiency, therefore, the optimizing function $F(x)$ is described the cost and efficiency through weighting factors as following

$$F(x) = k_1 F_1(x) + k_2 \eta_2(x) \quad (5)$$

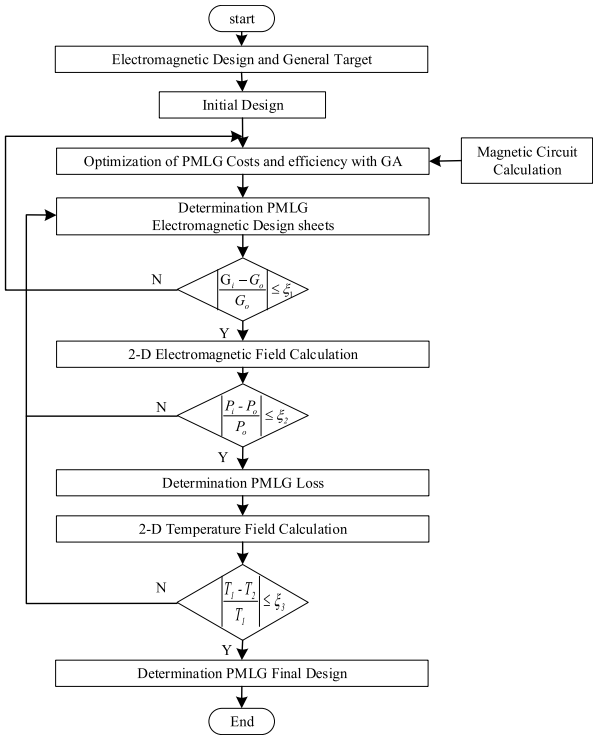

FIGURE 6. Optimization flow diagram for PMLSG.

where k_1 and k_2 are the cost and efficiency coefficient, respectively. $F_1(x)$ and $F_2(x)$ are the cost and efficiency objective functions.

The costs mainly include the PMs, windings, primary and secondary cores, and the processing costs. The costs of material are related to the weight and prices. The cost objective function can be written as

$$F_1(x) = k_{Fe} \times W_{Fe} + k_{Cu} \times W_{Cu} + k_{PM} \times W_{PM} + k_{pro} \times C_{pro} \quad (6)$$

where k_{Fe}, k_{Cu}, and k_{PM} are unit prices of silicon steel, copper, and permanent magnet, respectively. W_{Fe}, W_{Cu}, and W_{PM} are the weight of silicon steel, copper, and permanent magnet, respectively. k_{pro} is the unit coefficient processing, and C_{pro} is unit processing costs.

The efficiency of three phase PMLSG is other important parameter that can describe the electromagnetic performance of PMLSG, and it also one of the optimized targets. The mathematical expression of PMLSG is as follows

$$\eta_2(x) = \frac{P_o}{P_i} \times 100\% = \frac{3 \times U_o \times I_o}{3 \times U_o \times I_o + P_{Cu} + P_{Hy} + P_{Fe}} \times 100\% \quad (7)$$

where U_o and I_o are the Root Mean Square (RMS) of voltage and current, respectively. P_{Cu}, P_{Hy}, and P_{Fe} are the copper loss, hysteresis loss, and core loss, respectively.

B. THERMAL ANSLYSIS MODEL

The primary objective of the established thermal model is to estimate the permanent magnet temperature to avoid demagnetization. The thermal model is a nodal network [20] and which is shown in Fig. 7. P_{iron}, P_m, and P_{cu} are the iron loss, permanent magnet loss, and copper loss, respectively. Airgap flows are considered only in the direction axial to the airgap. A temperature source (T_{amb}) is a fixed temperature which equivalent to the current source of the electrical circuit.

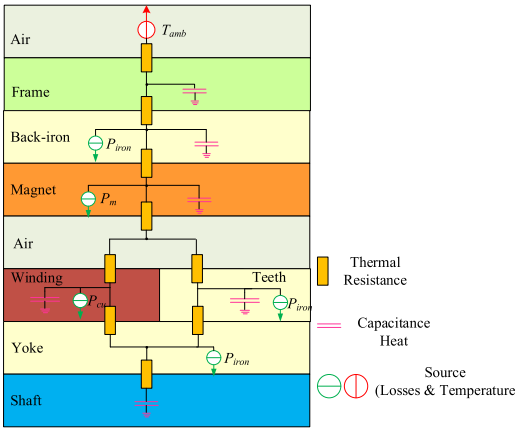

FIGURE 7. Nodal network for PMLSG.

1) LOSS CALCULATION

In the thermal analysis model, the mainly heat generation is copper loss and which is much higher than the iron loss. Among them, the simplified calculation of copper loss is,

$$P_{Cu} = mI^2R \tag{8}$$

where m is the number of phases of the generator, I is the effective value of current, R is the resistance of each phase and value is rise associates with the temperature.

The iron loss composes of two parts: hysteresis loss and eddy-current loss. The trend of the magnetic flux is nearly sinusoidal for the designed generator. Therefore, it can be calculated according to electromagnetism analysis [21].

$$P_{Fe} = K_h f B_m^{\beta} + K_e (f B_m)^2 \tag{9}$$

where B_m and f are the amplitude and frequency of the flux density, respectively. K_h and K_e are the hysteresis and eddy-current constants, and β is Steinmetz constant. Since the designed generator is mainly used in low speed applications, such as wave power take-off system, its frequency often below 10 Hz. Therefore, the eddy-current loss is ignored in the process of design.

2) THERMAL COEFFICIENTS

The conductive heat transfer coefficient (λ) value is related to the temperature of the material. The material conducts heat decreases with the λ increase. The contact heat transfer coefficient (k) has an impact on imperfect contact between two areas,. Due to the influence of fluid field, it is difficult to determine the coefficient of heat dissipation and heat transfer. In this paper, the designed PMLSG is applied to wave energy conversion, and PMLSG is often moving at low speeds, therefore, the air-cooled is selected.

In the two-dimensional Cartesian coordinate system, the transient heat conduction equation is given as following,

$$\rho c \frac{\partial T}{\partial t} = \lambda \left(\frac{\partial^2 T}{\partial x^2} + \frac{\partial^2 T}{\partial y^2} \right) + q_v \tag{10}$$

where ρ, c, and λ are the density of material, the material's specific heat capacity, and the material's conductivity, respectively. T is the node temperature, and q_v is the heat generation per unit.

The value of the convective heat transfer coefficient (h) is determined by the dimensionless Nusselt number (N_u), and the value is often calculated by a function with Prandtl (P_r), Reynolds number R_e, and Grashof number G_r. The convective heat transfer coefficient is calculated as following formula,

$$h = \frac{\lambda N_u}{L_g} \tag{11}$$

$$R_e = \frac{\rho v D}{\mu} \tag{12}$$

$$P_r = \frac{\mu c}{\lambda} \tag{13}$$

$$G_r = \frac{g \alpha \Delta T l_g^3}{v^2} \tag{14}$$

where L_g is the characteristic of the airgap, D is the hydraulic diameter of the air gap. μ, v,, ρ and g are the viscosity, velocity,, density of the air and acceleration of gravity, respectively. α is the volume expansion coefficient. $\Delta T = T_s - T_f$, Ts is the surface temperature, and T_f is the fluid temperature.

The air-cooled convection includes two kinds, that is the forced air-cooled convection coefficient (h_1) which is related to speed of PMLSG, and natural air-cooled convection coefficient (h_2).

The air flow type is laminar flow for forced air-cooled convection because of the value of R_e does not exceed 3×10^5. The forced air-cooled convection coefficients for the upper surfaces [N_{ux}] and lateral sides of the stator [N_{uD}] are given in the following [20], [22].

$$N_{ux} = \frac{h_x x}{\lambda_g} = 0.332 R_e^{1/2} P_r^{1/3} \tag{15}$$

$$N_{uD} = \frac{hD}{\lambda_g} = 0.16 R_{eD}^{0.699} \tag{16}$$

For linear generator, which is employed in wave power generation system, which is always works under reciprocating condition. The parameter h_1 is related with the air flow velocity. Through investigation, the velocity of wave is about 0.5 m/s-1 m/s at the experimental site. Therefore, the velocity is chosen 1 m/s in the process of calculating the forced air-cooled convection coefficient.

The natural air-cooled convection coefficients are given in the following [20].

For the upper surface of back-iron

$$N_u = \frac{hl}{\lambda_g} = 0.54(G_r P_r)^{1/4} \tag{17}$$

For the lower surface of back-iron

$$N_u = \frac{hl}{\lambda_g} = 0.58(G_r P_r)^{1/5} \tag{18}$$

For the vertical side surface of back-iron

$$N_u = \frac{hl}{\lambda_g} = \left\{ 0.825 + \frac{0.387(G_r P_r)^{1/6}}{[1 + (\frac{0.492}{P_r})^{9/16}]^{8/27}} \right\}^2 \tag{19}$$

The natural air-cooled convection has little effect on the heat dissipation, therefore, the parameter h_2 almost has no effect on the temperature. Considering the working environment of PMLSG, the natural air-cooled convection coefficient ($h2$) can be set as constant.

3) COMPONENTS OF THE NODAL THERMAL NETWORK

The role of thermal resistances is to let the heat flow circulate from one node to another, and the thermal resistances composed of conductive, convective, and contact thermal resistance.

Conductive heat resistance occurs in both solid and stationary gaseous parts and which is calculated as following

$$R_{cd} = \int_0^l \frac{dx}{\lambda(x)A(x)} \tag{20}$$

where l and $A(x)$ are the length and area of solid and gaseous, respectively.

Contact thermal resistance is the imperfect contact between two adjacent solid areas, and which is calculated as following

$$R_{su} = \frac{1}{kA(x)} \tag{21}$$

The intervention of gas with a movement of mass which produced convective thermal resistance, and it is calculated as following

$$R_{cv} = \frac{1}{hA(x)} \tag{22}$$

During transient phenomena, the capacitance heats quantify the ability of the material to restore and absorb energy, and its value depends on the mass heat capacitance (c_p). For simplicity, it considered linearly on temperature. The calculation is performed by the following formula

$$C = c_p(T) \times M \tag{23}$$

where M is the mass of the material.

4) THERMAL ANALYSIS

According to the above analysis, the temperature rise of each nodal thermal network is calculated as following [18]

$$[C]\frac{d[T]}{dt} + [G][T] = [P] \tag{24}$$

where $[C]$ is the matrix of thermal capacitance, $[T]$ is the temperature rise of each nodal, [G] is the thermal conductance matrix, and $[P]$ is the power loss vector.

IV. RESULTS AND DISCUSSIONS

The GA method is adopted to optimize the parameters which is described in section III, and the goal of optimization is achieved the minimum cost and the efficiency which are expressed by (6) and (8). The sensitivity analysis [23] is used to reduce the computational time. Therefore, some parameters of the PMLSG have been assumed constant values such as the number slots, the number of pole pairs, and the phases. The results of the optimization method were verified by finite element analysis (FEA).

A. FLUX DENSITY

The material of stator and back-iron is chosen B50AR300, and the B-H curve which is provided by the manufacturer is shown in Fig. 8. Therefore, the maximum flux density in the stator teeth and back-iron is low 1.8 T in the process of design. On the one hand ensure that the silicon steel sheet is not magnetic saturation, and the other hand make sure that the temperature of the motor does not exceed the set value 80°C. Fig. 9 and 10 show the distribution of magnetic flux density of the optimized model with 30 Ω load condition at 1 m/s and 2 m/s, respectively. As can be seen from the figure, the maximum value of flux density are 1.46 T and 1.58 T at the stator. The value of flux density in the speed of 2 m/s is higher than in the speed of 1 m/s. Fig. 11 shows the distribution of magnetic field, and (a) and (b) are the overall and partial enlarged, respectively.

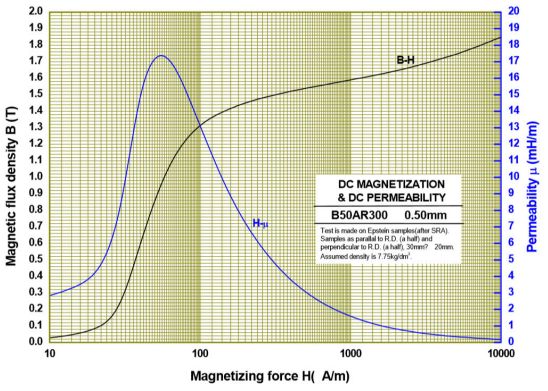

FIGURE 8. *B-H* and *H-μ* curve for B50AR300.

B. THERMAL ANALYSIS

In order to verify the above analysis, a transient thermal model of PMLSG is established by using FEA. The initial

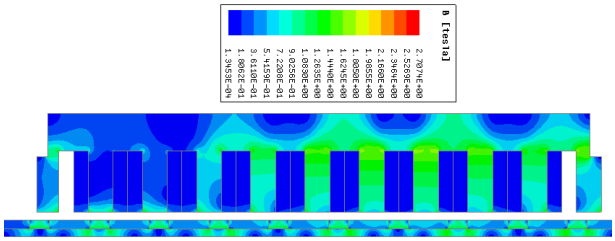

FIGURE 9. Flux densities at 1 m/s, 30 Ω.

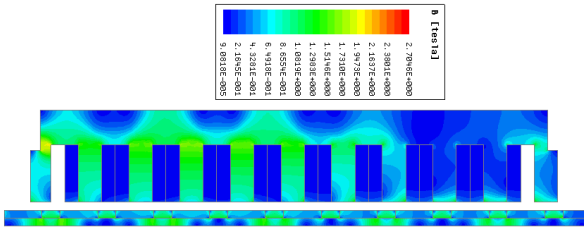

FIGURE 10. Flux densities at 2 m/s, 30 Ω.

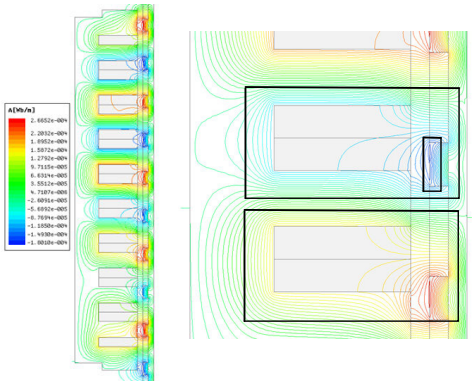

(a) overall (b) partial enlarged

FIGURE 11. Distribution of magnetic field.

temperature is 22 °C, and the heat generations are copper losses of windings, iron losses of stator and back-iron, and hysteresis losses of PMs. The calculated value of (15) and (16) bring into the equation (11), and get the value of heat transfer coefficient in the state of forced convention. Likewise, the heat transfer coefficient can be calculated by equation (17) to (19) and (11) in the state of natural convention. The heat transfer coefficients change greatly in the range of about 4-12 W/(m^2·K) and 40-65 W/(m^2·K) in the state of natural and forced convention [24]. The value of heat transfer coefficients slight increase with the time, the reason causing the phenomena is that the temperature rises of the surfaces.

The results of the electromagnetic field calculation are imported into the transient thermal analysis model, and the magnetic-thermal coupling analysis model is established by finite element analysis (FEA). Fig. 12 shows the temperature rise curves of coils, stator, permanent magnet (PM), and back-iron at 1 m/s and 30 Ω load. Among them, the temperature value of coils is largest, and the temperature

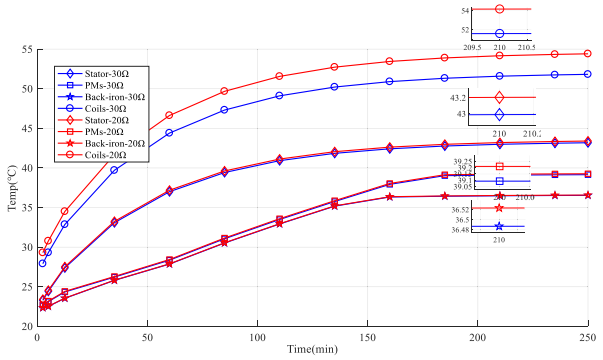

FIGURE 12. Temperature rise curves at 1 m/s, 30 Ω and 20 Ω load.

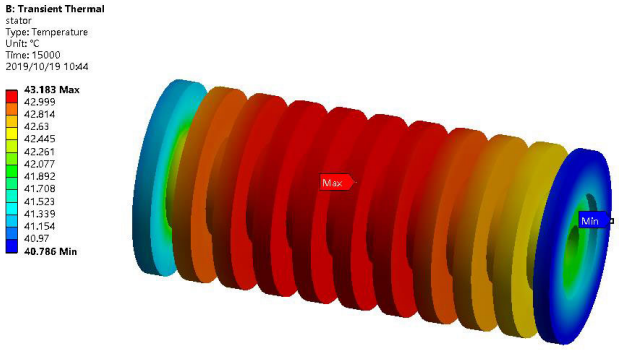

FIGURE 13. FEA calculated result of temperature for stator at 1 m/s.

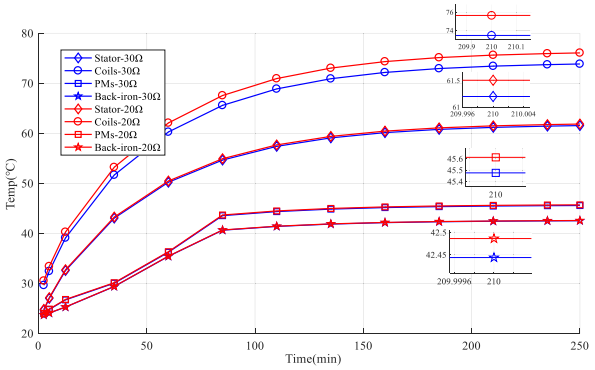

FIGURE 14. Temperature rise curves at 2 m/s, 30 Ω and 20Ω load.

value of back-iron is smallest. The temperature values of coils and back-iron have relatively large because the length of air-gap which reaches to 3 mm which can play a good heat dissipation. The value of temperature is basically stable while 135 minutes. As can be seen from the figure that the temperature increases as the time increases. Fig. 13 shows the temperature of stator at 1 m/s which works 250 minutes, and the maximin value is 43.183 °C. The temperature of stator in the middle is a little higher than the both ends, and the main reason is that the convection coefficients at both ends is higher than the middle. Fig. 14 shows the temperature rise curve of coils, stator, permanent magnet (PM), and back-iron at 2 m/s and 30 Ω load. Obviously, the value is significantly higher

TABLE 3. Compared performances with initial design.

	speed	P_{Fe} (W)	P_{Cu} (W)	P_{out} (W)	η (%)	Average Force (N)	Force ripple (%)
1 m/s	Initial	18.42	3.56	114.65	83.91	113.25	±26.25
	Optimized	20.22	4.22	246.32	90.86	128.42	±3.45
2 m/s	Initial	37.42	8.56	398.54	88.66	200.02	±28.43
	Optimized	39.19	8.87	467.46	90.68	244.97	±3.23

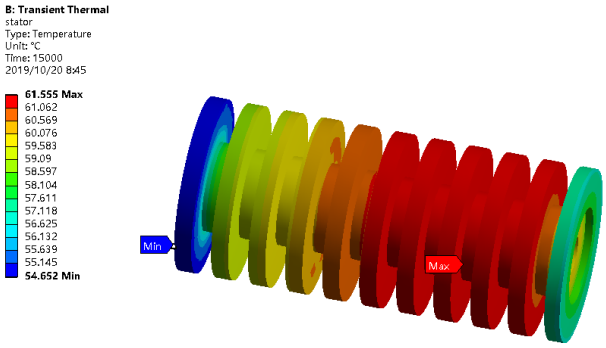

FIGURE 15. FEA calculated result of temperature for stator at 2 m/s.

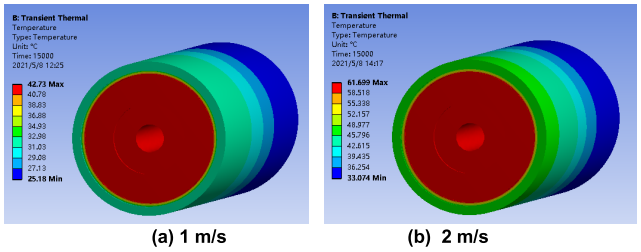

(a) 1 m/s (b) 2 m/s

FIGURE 16. FEA calculated result of overall temperature for PMLSG.

than under the working conditions of 1 m/s. The reason is that both the iron losses and copper losses at 2 m/s are higher than 1 m/s working conditions, and the losses are released as heat energy. Fig. 15 shows the temperature of stator at 2 m/s which also works 250 minutes, and the maximin value is 61.555°C. The temperature does not exceed the safe temperature. Fig. 16 shows the overall temperature of PMLSG. As can be seen from the figure, the maximum temperature is located at the coils and stator position. The results show that all the component parts are the allowable temperature range.

C. PERFORMANCE ANALYSIS

According to the above optimization analysis, the final optimized model is achieved. The optimized performances are evaluated and compared with the initial design, and the detail performances are shown in Table 3. The PMLSG is in the same working conditions, that is the load is 30 Ω, and the speed is 1 m/s and 2 m/s. As can be seen from the table, the electromagnetic performances are greatly improved after optimization. The force ripple is expresses in table 3 as following,

$$Force\ ripple = \frac{Force_{\max} - Force_{\min}}{Force_{ave}} \times 100\% \qquad (25)$$

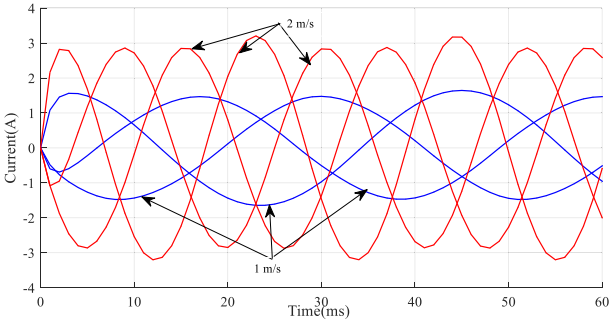

FIGURE 17. Current waveforms at 1 m/s and 2 m/s.

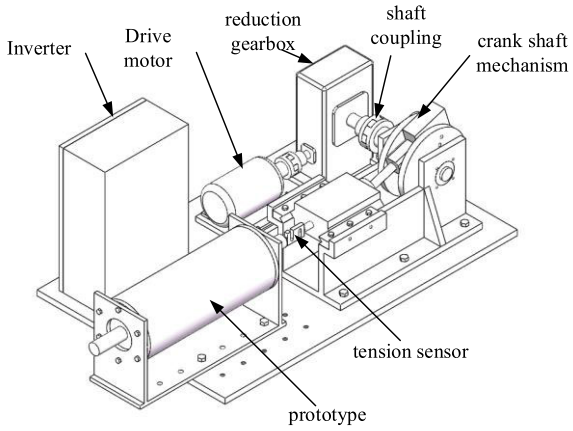

FIGURE 18. Structure diagram of the test system.

TABLE 4. Total harmonic distortion.

speed	THD (A phase)	THD (B phase)	THD (C phase)
1 m/s	0.28%	1.08%	0.99%
2 m/s	0.43%	0.87%	0.81%

where $Force_{max}$, $Force_{min}$, and $Force_{ave}$ are maximum force, minimum force, and average force, respectively.

Fig. 17 shows the current waveform under the load 30 Ω and speed 1 m/s and 2 m/s conditions. The total harmonic distortion is shown in table 4, From the table, it can be seen that the current waveform is sinusoidal.

V. TEMPERATURE TEST

The temperature test platform for PMLSG has been set up in order to verify the validity of the above analysis. The structure diagram of the test system is shown in the figure 18. It is composed mainly of inverter, drive motor,

FIGURE 19. Temperature test platform for PMLSG.

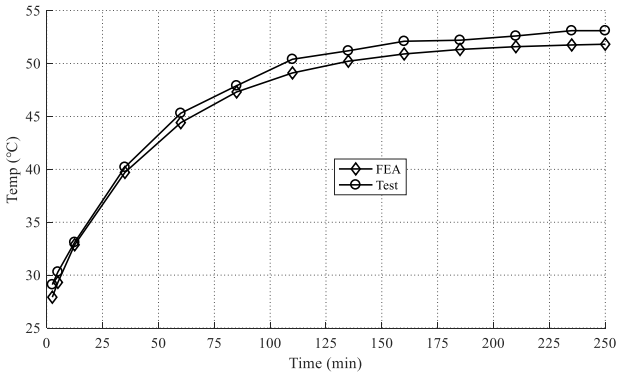

FIGURE 20. Temperature rise of coils at 1 m/s.

reduction gearbox, crank, tension, and prototype. The drive motor adopts a three-phase two-pole variable frequency asynchronous motor, which drives the crankshaft mechanism after being decelerated by the reduction gearbox. The stroke of the crankshaft connecting mechanism is 200mm, and the movement speed of the PLLSG is controlled by adjusting the frequency of the frequency converter. The test platform of PMLSG is shown in Fig. 19. Platinum thermistor which is embedded in coils is used to test the coils temperature. The speed of PMLSG is 1 m/s and 2 m/s by controlling the speed of drive motor. The generator work continuously for 250 minutes.

Fig. 20 and Fig. 21 show the coils temperature rise curve of the coils test and FEA at 1 m/s and 2 m/s, respectively. As we can be seen that the trends of FEA and test are almost same. The maximum temperatures of coils are 51.8 °C and 73.9 °C at 1 m/s and 2 m/s, respectively. The temperature of generator is a constant after working 135 min. The value of test is slightly higher than the FEA. This change is chiefly due to the following reasons:

1) The eddy current loss is ignored in the course of FEA. The purpose of this generator is employed in wave power generation, and the generator always works at low speed. The working frequency is low and below power frequency, so the

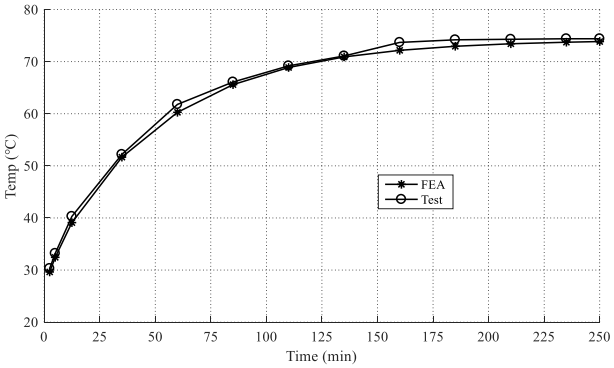

FIGURE 21. Temperature rise of coils at 2 m/s.

eddy current is far less than the copper losses and core losses. In fact, the eddy current loss will affect the temperature of the generator.

2) The friction loss is also ignored in the progress of FEA. The friction loss has related to the friction coefficient which corresponding to the precision of machining.

3) The temperature of generator is affected by the environmental temperature. The environmental temperature is changed, and always hard to maintain as a constant value.

VI. CONSLUSION

In this paper, a multi-physical coupling field of PMLSG which is employed in a low speed condition is presented to improve the utilization of the materials and efficiency. The GA optimization method is applied to optimize the performance of PMLSG, and the results are validated by experimental results. From the above calculations and experiment, the following results can be obtained.

1) Considering the characteristics of wave motion, the multidisciplinary design model is established, and the multi-objective optimization method base on GA is employed to optimize the parameters.

2) The electromagnetic analysis model is established according to the optimized parameters, and the electromagnetic parameters and loss values are import the magnetic-thermal coupling model. The temperature rise of the stator, coils and other component are calculated. The heat transfer coefficients for the stator, coils, PMs and secondary are calculated using the temperature calculation result of the air-gap thermal circuit as the condition. Simulation and experimental results show that the designed PMLSG can be applied to wave energy conversions.

3) An experiment test platform is set up to verify the analysis results, and the test results are good agreement with the calculated results.

REFERENCES

[1] Z. Liu, X. Wang, E. Al Shami, N. J. Baker, and X. Ji, "A study of a speed amplified linear generator for low-frequency wave energy conversion," *Mech. Syst. Signal Process.*, vol. 149, Feb. 2021, Art. no. 107226.

[2] S. Rasool, M. R. Islam, K. M. Muttaqi, and D. Sutanto, "Coupled modeling and advanced control for smooth operation of a grid-connected linear electric generator based wave-to-wire system," *IEEE Trans. Ind. Appl.*, vol. 56, no. 5, pp. 5575–5584, Sep. 2020.

[3] L. Drazikowski and B. Kaminski, "Coreless linear permanent magnet synchronous machine as a direct servo drive for CNC milling machine," *Przeglad Elektrotechniczny*, vol. 86, no. 2, pp. 131–135, 2010.

[4] N. Simpson, R. Wrobel, and P. H. Mellor, "A multiphysics design methodology applied to a high-force-density short-duty linear actuator," *IEEE Trans. Ind. Appl.*, vol. 52, no. 4, pp. 2919–2929, Jul. 2016.

[5] Z. Yao, J. Zhao, J. Song, F. Dong, Z. He, and K. Zong, "Research on selection criterion of design tolerance for air-core permanent magnet synchronous linear motor," *IEEE Trans. Ind. Electron.*, vol. 68, no. 4, pp. 3336–3347, Apr. 2021.

[6] F. Dong, J. Zhao, J. Song, J. Zhao, and Z. Yao, "Robust design optimization of permanent magnet linear synchronous motor based on quantified constraint satisfaction problem," *IEEE Trans. Energy Convers.*, vol. 35, no. 4, pp. 2013–2024, Dec. 2020.

[7] F. Grimaccia, G. Gruosso, M. Mussetta, A. Niccolai, and R. E. Zich, "Design of tubular permanent magnet generators for vehicle energy harvesting by means of social network optimization," *IEEE Trans. Ind. Electron.*, vol. 65, no. 2, pp. 1884–1892, Feb. 2018.

[8] F. Dong, J. Zhao, J. Song, Y. Feng, and Z. He, "Optimal design of permanent magnet linear synchronous motors at multispeed based on particle swarm optimization combined with SN ratio method," *IEEE Trans. Energy Convers.*, vol. 33, no. 4, pp. 1943–1954, Dec. 2018.

[9] C. Liu, H. Gao, Y. Xiong, S. Zhou, and W. Fu, "Detent force reduction in permanent magnet linear synchronous motor base on magnetic field similarity method," *IEEE Access*, vol. 7, pp. 57341–57348, 2019.

[10] H. Hu, X. Liu, J. Zhao, and Y. Guo, "Analysis and minimization of detent end force in linear permanent magnet synchronous machines," *IEEE Trans. Ind. Electron.*, vol. 65, no. 3, pp. 2475–2486, Mar. 2018.

[11] B. Zhang, M. Cheng, J. Wang, and S. Zhu, "Optimization and analysis of a yokeless linear flux-switching permanent magnet machine with high thrust density," *IEEE Trans. Magn.*, vol. 51, no. 11, Nov. 2015, Art. no. 8204804.

[12] O. Wallscheid and J. Bocker, "Global identification of a low-order lumped-parameter thermal network for permanent magnet synchronous motors," *IEEE Trans. Energy Convers.*, vol. 31, no. 1, pp. 354–365, Mar. 2016.

[13] J. Doering, G. Steinborn, and W. Hofmann, "Torque, power, losses, and heat calculation of a transverse flux reluctance machine with soft magnetic composite materials and disk-shaped rotor," *IEEE Trans. Ind. Appl.*, vol. 51, no. 2, pp. 1494–1504, Mar. 2015.

[14] L. N. Li, W. N. Fu, S. L. Ho, S. X. Niu, and Y. Li, "A quantitative comparison study of power-electronic-driven flux-modulated machines using magnetic field and thermal field co-simulation," *IEEE Trans. Ind. Electron.*, vol. 62, no. 10, pp. 6076–6083, Oct. 2015.

[15] F. Marignetti, V. Delli Colli, and Y. Coia, "Design of axial flux PM synchronous machines through 3-D coupled electromagnetic thermal and fluid-dynamical finite-element analysis," *IEEE Trans. Ind. Electron.*, vol. 55, no. 10, pp. 3591–3601, Oct. 2008.

[16] J. Wang and D. Howe, "Tubular modular permanent-magnet machines equipped with quasi-Halbach magnetized magnets—Part I: Magnetic field distribution, EMF, and thrust force," *IEEE Trans. Magn.*, vol. 41, no. 9, pp. 2470–2478, Sep. 2005.

[17] J. Luomi, C. Zwyssig, A. Looser, and J. W. Kolar, "Efficiency optimization of a 100-W 500 000-r/min permanent-magnet machine including air-friction losses," *IEEE Trans. Ind. Appl.*, vol. 45, no. 4, pp. 1368–1377, Jul./Aug. 2009.

[18] W. Li, P. Wang, D. Li, X. Zhang, J. Cao, and J. Li, "Multiphysical field collaborative optimization of premium induction motor based on GA," *IEEE Trans. Ind. Electron.*, vol. 65, no. 2, pp. 1704–1710, Feb. 2018.

[19] C. Sciascera, P. Giangrande, L. Papini, C. Gerada, and M. Galea, "Analytical thermal model for fast stator winding temperature prediction," *IEEE Trans. Ind. Electron.*, vol. 64, no. 8, pp. 6116–6126, Aug. 2017.

[20] Q. Lu, X. Zhang, Y. Chen, X. Huang, Y. Ye, and Z. Q. Zhu, "Modeling and investigation of thermal characteristics of a water-cooled permanent-magnet linear motor," *IEEE Trans. Ind. Appl.*, vol. 51, no. 3, pp. 2086–2096, May 2015.

[21] C. Mi, G. R. Slemon, and R. Boner, "Modeling of iron losses of permanent-magnet synchronous motors," *IEEE Trans. Ind. Appl.*, vol. 39, no. 3, pp. 734–741, May/Jun. 2003.

[22] H. Li and Y. Shen, "Thermal analysis of the permanent-magnet spherical motor," *IEEE Trans. Energy Convers.*, vol. 30, no. 3, pp. 991–998, Sep. 2015.

[23] C. Liu, H. Zhu, R. Dong, S. Zhou, and L. Huang, "Sensitivity analysis and optimal design of a linear magnetic gear for direct-drive wave energy conversion," *IEEE Access*, vol. 7, pp. 73983–73992, 2019.

[24] X. Huang, L. Li, B. Zhou, C. Zhang, and Z. Zhang, "Temperature calculation for tubular linear motor by the combination of thermal circuit and temperature field method considering the linear motion of air gap," *IEEE Trans. Ind. Electron.*, vol. 61, no. 8, pp. 3923–3931, Aug. 2014.

CHUNYUAN LIU received the Ph.D. degree from Southeast University, Nanjing, China, in 2015. He is currently an Assistant Professor with the College of Information Science and Engineering (College of Mechanical Engineering), Jiaxing University, China. His current research interests include design and control of novel electrical machines and drives, renewable energy conversion systems, and applied electromagnetics.

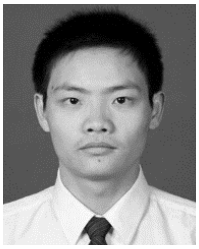

DONG RUI received the M.S. degree in electrical engineering from the Wuhan University of Technology, China, in 2010. He has been a Lecturer with the College of Information Science and Engineering (College of Mechanical Engineering), Jiaxing University. His research interests include power electronics equipment, drive of PMSM, and linear motor.

HE ZHU was born in Harbin, China, in 1979. He received the B.S. degree in computer science and technology from the Harbin Institute of Technology (HIT), Harbin, the M.S. degree in power system and its automation from Harbin Engineering University, and the Ph.D. degree in electrical machines and electrical apparatus from HIT, in 2015. He is currently a Lecturer with the College of Information Science and Engineering (College of Mechanical Engineering), Jiaxing University. His research interests include electric motor drive and control systems, especially in the fields of AC electromotor/generator control and driving technology, PM synchronous motor servo control systems, sensorless control, and industrial automation.

WENZHEN FU received the M.S. degree in electrical engineering and automation from the South China University of Technology, in 2009. His research interests include wireless energy transmission, designed and implemented of switching power supply, and the application of micro inverter in photovoltaic systems.